Distinct evolution of the carbonaceous and non-carbonaceous reservoirs: Insights from Ru, Mo, and W isotopes

Emily A. Worsham [a,*], Christoph Burkhardt [a], Gerrit Budde [a], Mario Fischer-Gödde [a,b], Thomas S. Kruijer [c], Thorsten Kleine [a]

[a] *Institut für Planetologie, University of Münster, Wilhelm-Klemm-Str. 10, 48149 Münster, Germany*
[b] *Institut für Geologie und Mineralogie, University of Köln, Zülpicherstrasse 49, 50923 Köln, Germany*
[c] *Lawrence Livermore National Laboratory, Livermore, CA 94550, USA*

ARTICLE INFO

ABSTRACT

Recent work has identified a nucleosynthetic isotope dichotomy between "carbonaceous" (CC) and "non-carbonaceous" (NC) meteorites. Here, we report new Ru isotope data for rare iron meteorite groups belonging to the NC and CC suites. We show that by studying the relative isotopic characteristics of Ru, Mo, and W in iron meteorites, it is possible to constrain the processes leading to the distinct isotope heterogeneities in both reservoirs. In NC meteorites, internally normalized, mass-independent isotope ratios of Mo and Ru are correlated, but those of Mo and W are not. In CC meteorites, Mo and W isotope ratios are correlated, but those of Mo and Ru are not; specifically, Mo isotopic compositions are variable and those of Ru are more restricted. The contrasting behaviors of Ru and W relative to Mo in the two reservoirs likely require processing of the presolar carriers under distinct redox conditions. This provides further evidence that NC and CC meteorites originated from spatially separated reservoirs that evolved under different prevailing conditions.

© 2019 Elsevier B.V. All rights reserved.

1. Introduction

The current structure of the solar system, i.e., terrestrial planets in the inner solar system and gaseous giants and icy moons in the outer solar system, resulted from the formation of chemical reservoirs early in the evolution of the protoplanetary disk. In recent decades, isotopic reservoirs have also been identified by the presence of nucleosynthetic isotope anomalies in most elements in bulk meteorites, which likely reflects the heterogeneous distribution of isotopically diverse presolar materials in the early protoplanetary disk (see summary in Dauphas and Schauble, 2016). These nucleosynthetic isotope anomalies are small (typically identified at the parts per 10^4-10^6 level), mass-independent, and are representative of the unique mixtures of presolar materials in the various nebular reservoirs from which planetary bodies accreted. By contrast, some elements, including Os and Pt, display no nucleosynthetic heterogeneity in bulk meteorites at the current level of precision (with few exceptions – Goderis et al., 2015), indicating that the solar nebula may have been initially isotopically homogeneous, or that these elements were hosted in homogeneously distributed carriers (e.g., Walker, 2012; Kruijer et al., 2013). Considering this hypothesized initial homogeneity, the origin of the heterogeneous distribution of presolar materials and, thus, the origin of nucleosynthetic anomalies remains ambiguous. Some proposed mechanisms involve inefficient mixing of presolar materials, resulting in inherited heterogeneities in the solar nebula (Clayton, 1982; Dauphas et al., 2002a), grain type- or size-sorting (Regelous et al., 2008; Dauphas et al., 2010), or thermal processing of unstable presolar phases (Trinquier et al., 2009).

Another facet of nucleosynthetic heterogeneity is the recent identification of a major isotopic dichotomy among meteorites in several elements, including Ti, Cr, Mo, W, Ru, and Ni (Warren, 2011; Budde et al., 2016; Kruijer et al., 2017; Poole et al., 2017; Worsham et al., 2017; Bermingham et al., 2018; Nanne et al., 2019). Carbonaceous chondrites, several iron meteorite groups, and some ungrouped irons and achondrites fall into the "carbonaceous" (CC) suite. The "non-carbonaceous" (NC) suite is comprised of ordinary and enstatite chondrites and all other iron meteorite groups and achondrites measured thus far. Broadly speaking, CC meteorites have elevated abundances of nuclides synthesized in neutron-rich stellar environments (including *r*-process Mo isotopes), relative to NC meteorites. The presence of both irons, which have older estimated accretion ages, and chondrites, which have younger accretion ages, in both suites indicates that they repre-

* Corresponding author.
E-mail address: worsham@uni-muenster.de (E.A. Worsham).

sent different nebular reservoirs that were spatially distinct, and that the reservoirs remained separated for several Ma (Budde et al., 2016; Kruijer et al., 2017). Kruijer et al. (2017) suggested that the reservoirs were separated due to the growth of Jupiter's core. In this case, the NC and CC reservoirs represent the inner and outer solar system, suggesting that the conditions that affected presolar carriers in each reservoir may have been different.

To investigate the generation of nucleosynthetic variations among the various nebular reservoirs, we utilize the relative isotopic characteristics of Mo, Ru, and W in iron meteorites. These elements are useful because they have distinct physicochemical behaviors under different nebular conditions. Further, Mo, Ru, and W are created by a combination of *p*-process, *s*-process, and *r*-process nucleosynthesis. Therefore, these elements are ideal tracers of diverse nucleosynthetic signatures in solar system materials. We report new Ru isotope data for magmatic iron meteorite groups belonging to both the NC (IC and IIIE) and CC suites (IIC, IID, IIF, and IIIF), for most of which no Ru isotope data have been reported before. In conjunction with Mo and W isotope data, the Ru data provide new constraints on the various processes and environmental conditions that led to the isotope heterogeneities within the NC and CC reservoirs.

2. Analytical methods

2.1. Samples

The samples used to obtain Ru isotope data were predominately adjacent pieces of the same samples that were used to obtain Mo, W, and Pt isotope data in the study of Kruijer et al. (2017). Additional samples were incorporated into this study, for which Ru and Mo isotope data (and sometimes Pt) were obtained from aliquots of the same digestion. Platinum was used as a neutron fluence dosimeter to monitor for the effects of cosmic ray exposure (CRE), which can modify the isotopic compositions of Ru, Mo, and W (Kruijer et al., 2013; Fischer-Gödde et al., 2015; Worsham et al., 2017).

2.2. Chemical purification procedures

A detailed description of the purification procedures is given in the supplementary material (SM). Briefly, iron meteorite samples between 0.3 and 0.6 g were digested in Teflon beakers in 6 M HCl with traces of HNO_3. Ruthenium was separated from the matrix using cation exchange chromatography and was purified via micro-distillation (Birck et al., 1997; Fischer-Gödde et al., 2015). After purification of Ru, Mo/Ru and Pd/Ru were always $<1 \times 10^{-5}$. Molybdenum was separated and purified using a three-stage cation and anion exchange chromatographic procedure, including a Truspec column to remove Ru (Burkhardt et al., 2011). The Zr/Mo and Ru/Mo after this chemistry was typically $<5 \times 10^{-5}$. Platinum was separated using a single-stage anion exchange chromatography procedure (Method 1; Rehkämper and Halliday, 1997). Given that the concentrations of Mo, Ru, and Pt are high in the iron meteorites studied here, the total analytical blanks were negligible (<1 ng for Ru and Pt, <10 ng for Mo).

2.3. Mass spectrometry

Ruthenium, Mo, and Pt analyses were conducted using a *Thermo Scientific Neptune Plus* multi-collector inductively coupled plasma mass spectrometer (MC-ICP-MS) at the Institut für Planetologie, University of Münster. Ion beams were collected simultaneously using Faraday cups for 100 cycles. Molybdenum-97 and ^{105}Pd, ^{91}Zr and ^{99}Ru, and ^{189}Os and ^{200}Hg were used to monitor and correct for interferences on Ru, Mo, and Pt, respectively. The Ru,

Mo, W, and Pt isotopic compositions are reported in ε notation (parts-per-10^4 deviations from terrestrial standards). Interference corrections for ε^{100}Ru were typically $<0.1\varepsilon$, usually on the order of a few ppm. For ε^iMo interference corrections were $<1\varepsilon$, usually on the order of 10s of ppm. The data are normalized to ^{99}Ru/^{101}Ru, ^{98}Mo/^{96}Mo, ^{186}W/^{184}W, and ^{198}Pt/^{195}Pt. Based on previous studies from our lab, and monitored during this study, the external reproducibilities (2SD) of the repeated analyses of terrestrial standards for each element are ± 0.13 for ε^{100}Ru, ± 0.28 for ε^{94}Mo, ± 0.08 for ε^{183}W, and ± 0.07 for ε^{196}Pt.

3. Results

3.1. Effects of cosmic ray exposure on Ru and Mo isotopes

The CRE effects were monitored using Pt isotope data reported here and in Kruijer et al. (2017) (Table 1). These effects are dependent, in part, on the shielding depth of the sample, so samples used in this study typically came from within ~ 3 cm of the piece from which the Pt isotope data were obtained. The effects of CRE on Ru and Mo have been described by Fischer-Gödde et al. (2015), Worsham et al. (2017), and Bermingham et al. (2018). For Ru, the largest effects are on ε^{100}Ru. For Mo, in order of largest to smallest, the effects are on ε^{92}Mo, ε^{95}Mo $\approx \varepsilon^{94}$Mo, and ε^{97}Mo. Effects on ε^{100}Ru and ε^{94}Mo are similar in magnitude (i.e., ranging up to $\sim 0.5\ \varepsilon$ units, but typically $<0.15\ \varepsilon$).

Most samples used in this study have minimal CRE effects. Excluding the irons with the most significant effects (Arispe, Bendego, Murnpeowie, Kokstad, and Oakley), CRE results in $\leq 0.06\ \varepsilon$ changes in the ε^{100}Ru and ε^{94}Mo values, averaging 0.02 ε for both. Therefore, no CRE correction is necessary for either Ru or Mo for most samples, and we report uncorrected Ru and Mo isotope data and low-exposure averages for each iron meteorite group, incorporating only irons with ε^{196}Pt ≤ 0.13 (Tables 2, 3, and SM1; Figs. 1 and 2). Although unnecessary for most irons, CRE-corrected Ru data are given in Table SM2. Robust CRE corrections could not be done for Mo (see SM).

The use of uncorrected data is sufficient for the aims of this study, which is primarily concerned with isotopic differences between NC and CC groups. As shown in Figs. 1 and 2, these differences are larger than those expected to arise from unaccounted-for CRE effects. However, CRE effects should be corrected when Mo and Ru isotopes are used for genetic testing or where the precision and accuracy of isotopic correlations are important (Bermingham et al., 2018).

Weighted-average literature data for other meteorite groups are also shown on Fig. 1. For the major iron meteorite groups, the averages include CRE-corrected group means (Fischer-Gödde et al., 2015; Bermingham et al., 2018) and means of low-exposure irons from each group (Chen et al., 2010; Burkhardt et al., 2011; Poole et al., 2017) (Tables SM3 and SM4). The ^{183}W data do not require CRE correction (Kruijer et al., 2017).

3.2. Ru and Mo isotope results

The Ru and Mo data are reported in Tables 2 and 3. The highest precision is obtained for ε^{100}Ru, and the other ε^iRu values are of lower precision because they are of lower abundance (^{96}Ru and ^{98}Ru) or more difficult to measure precisely and accurately due to their distance in AMU from the normalizing ratio (^{96}Ru and ^{104}Ru). For this reason, and because ε^{100}Ru displays the most distinctive variations, only these values are presented here and discussed, although all Ru data are reported in Table SM1. Two pairs of duplicate analyses each for ε^{100}Ru and ε^{94}Mo reproduced well (within 7 ppm of one another). The only rare iron meteorite groups with previously reported Ru data

Table 1
Platinum isotope data used to monitor CRE effects.

Meteorite	Collection (No.)	N	ε^{192}Pt[a]	±	ε^{194}Pt	±	ε^{196}Pt	±
IC								
Chihuahua City[b]	BM 1959, 1011	1	0.50	1.30	0.17	0.11	0.07	0.07
Arispe[b]	Münster	6	13.33	0.27	0.52	0.03	0.35	0.03
Arispe (replicate)[b]	Münster	6	12.89	0.36	0.48	0.04	0.32	0.04
Arispe (replicate)[b]	ME 1011	3	13.69	1.30	0.67	0.11	0.42	0.07
Bendego	ME 6	4	0.62	1.00	0.37	0.06	0.49	0.06
Bendego (replicate)[b]	ME 6	3	1.08	1.30	0.32	0.11	0.47	0.07
Bendego (replicate)[b]	USNM #351	2	−0.57	1.30	0.38	0.11	0.52	0.07
Mount Dooling	USNM 5713	5	−0.39	0.98	0.07	0.05	0.00	0.03
Murnpeowie[b]	BM 2005, M179	2	3.95	1.30	0.50	0.11	0.38	0.07
Murnpeowie (replicate)[b]	BM 2005, M179	4	2.34	1.05	0.29	0.11	0.26	0.05
IIC								
Kumerina	BM 1938, 220	4	0.52	0.89	−0.02	0.05	−0.09	0.03
Kumerina (replicate)[b]	BM 1938, 220	2	0.80	1.30	0.17	0.11	0.04	0.07
Kumerina (replicate)[b]	BM 1938, 220	3	−0.02	1.30	0.04	0.11	−0.02	0.07
Perryville	USNM 428	5	2.14	1.12	0.16	0.05	0.05	0.05
Unter-Mässing	Münster	5	5.20	0.60	0.18	0.04	0.12	0.02
Ballinoo[b]	ME 980	3	−0.37	1.30	0.08	0.11	−0.01	0.07
Wiley	BM 1959, 914	5	0.97	0.45	0.04	0.07	0.01	0.02
Wiley (replicate)[b]	BM 1959, 914	4	0.55	1.34	0.12	0.05	0.05	0.07
Wiley (replicate)[b]	BM 1959, 914	5	0.58	0.65	0.11	0.06	0.08	0.06
IID								
Bridgewater[b]	ME 1895	5	0.80	0.90	0.02	0.08	−0.01	0.02
N'kandhla[b]	BM 1921, 17	5	0.64	0.23	0.03	0.05	0.01	0.05
IIF								
Monahans[b]	BM 1959, 910	4	0.91	0.90	0.15	0.05	0.07	0.04
Monahans (replicate)[b]	BM 1959, 911	2	1.43	1.30	0.09	0.11	0.08	0.07
Del Rio	USNM 6524	5	2.37	1.04	0.05	0.06	0.04	0.03
IIIE								
Willow Creek[b]	Münster	1	0.55	1.30	0.14	0.11	0.13	0.07
Kokstad[b]	ME 1015	1	1.62	1.30	0.38	0.11	0.35	0.07
Kokstad (replicate)[b]	ME 1015	2	0.82	1.30	0.29	0.11	0.26	0.07
Colonia Obreira[b]	ME 2871	1	0.17	1.30	0.06	0.11	−0.01	0.07
Colonia Obreira (replicate)[b]	ME 2871	1	−0.30	1.30	0.08	0.11	0.03	0.07
Staunton[b]	BM 1955, M239	1	−0.17	1.30	0.15	0.11	−0.07	0.07
Staunton (replicate)[b]	BM 1955, M239	2	−0.28	1.30	0.08	0.11	0.05	0.07
Paneth's iron[b]	BM 2005, M199	2	0.26	1.30	0.12	0.11	0.09	0.07
Burlington	USNM 978	3	0.17	1.30	0.18	0.11	0.07	0.07
Coopertown	USNM 1003	4	0.39	1.28	0.11	0.05	0.02	0.06
IIIF								
Klamath Falls[b]	ME 2789	1	0.39	1.30	0.06	0.11	0.06	0.07
Klamath Falls (replicate)[b]	ME 2789	1	0.99	1.30	0.13	0.11	−0.01	0.07
Clark County[b]	BM 1959, 949	4	2.81	0.78	0.08	0.06	0.03	0.07
Clark County (replicate)[b]	BM 1959, 949	2	3.54	1.30	0.17	0.11	0.10	0.07
Oakley	USNM 780	4	18.93	3.33	0.78	0.09	0.48	0.06

[a] Data are reported in epsilon notation $[(R_{sample}/R_{standard} - 1) \times 10{,}000]$, and normalized to ^{198}Pt/^{195}Pt $= 0.2145$. For the number of analyses of the same solution $N < 4$, the uncertainties are the 2SD of repeated analyses of solution standards. For $N \geq 4$, uncertainties are the 95% confidence interval of the mean, according to (SD × $t_{0.95,N-1}$)/$\sqrt{N}$.

[b] Data from Kruijer et al. (2017).

are the IC and IID groups, and the new data for those groups are in good agreement (Table SM5 – Fischer-Gödde et al., 2015; Bermingham et al., 2018).

The Mo isotope data are also in generally good agreement with previous studies (Table SM6 – Burkhardt et al., 2011; Poole et al., 2017; Bermingham et al., 2018). In detail, there are potentially small systematic offsets, primarily in ε^{92}Mo, between this study (and Kruijer et al., 2017) and the data reported by Poole et al. (2017) (Table SM6). Apart from the IIIE group, the ε^{92}Mo data reported by Poole et al. (2017) are within uncertainty of the data reported here but are generally higher by 0.2 to 0.3 ε for the IC, IIC, IIIE, and IIIF groups. Some of these offsets are likely due to the different exposure histories of the samples used in each study, but the systematic nature of the offsets would suggest this is not always the case. As the ε^{94}Mo and ε^{95}Mo values show no significant offsets, these data are used in the following discussion.

The Mo isotope dichotomy (Fig. 1) is partially defined by excess ^{95}Mo, relative to ^{94}Mo, in CC meteorites when compared to NC

meteorites, resulting in two parallel trends on a plot of ε^{94}Mo versus ε^{95}Mo (e.g., Budde et al., 2019). The Mo isotopic compositions indicate that the IC and IIIE groups belong to the NC suite, in addition to the IAB, IIAB, IIIAB, and IVA iron meteorite groups and the ordinary and enstatite chondrites (Fig. 1; Kruijer et al., 2017). The IIC, IID, IIF, and IIIF groups, in addition to the IVB iron group and carbonaceous chondrites, belong to the CC suite (e.g., Kruijer et al., 2017). In Fig. 1, only carbonaceous chondrite metals are shown, as Mo and Ru isotopic compositions obtained from separate digestions of bulk unequilibrated chondrites are not directly comparable due to the potential for incomplete digestion of presolar phases.

The new ε^{94}Mo and ε^{100}Ru data for IC, IIC, IID, IIF, IIIE, and IIIF irons are shown in Fig. 2, supplemented with Mo and W isotope data from Kruijer et al. (2017). Iron meteorites from the NC groups IC and IIIE have Mo and Ru isotopic compositions most like IIAB iron meteorites (ε^{94}Mo ~ 1.0; ε^{100}Ru ~ -0.5). Iron meteorites from the CC groups IID, IIF, and IIIF have Mo and Ru isotopic compositions similar to IVB irons and carbonaceous chondrite metals

Table 2

Ruthenium isotope data for rare iron meteorite groups. The data are not corrected for CRE exposure. Where groups include irons with ε^{196}Pt ≥ 0.13, a low-exposure mean excluding those irons is given. The excluded samples are denoted with an asterisk.

Meteorite	Collection (No.)	N	ε^{100}Ru[a]	±
IC				
Chihuahua City	BM 1959, 1011	5	−0.38	0.07
Arispe*	ME 1011	6	−0.24	0.05
Bendego*	ME 6	5	−0.16	0.10
Bendego (replicate)*	ME 6	2	−0.23	0.13
Mount Dooling	USNM 5713	5	−0.37	0.08
IC average			*−0.27*	*0.15*
Low exposure IC average			*−0.38*	*0.13*
IIC				
Kumerina	BM 1938, 220	5	−1.07	0.14
Perryville	USNM 428	5	−1.01	0.05
Unter-Mässing	Münster	5	−1.03	0.08
IIC average			*−1.04*	*0.05*
Wiley	BM 1959, 914	6	−1.10	0.10
Wiley (replicate)	BM 1959, 914	5	−1.04	0.13
Wiley average			*−1.07*	*0.08*
IID				
Bridgewater	ME 1895	5	−1.07	0.11
N'kandhla	BM 1921, 17	4	−1.02	0.13
IID average			*−1.04*	*0.13*
IIF				
Monahans	BM 1959, 910	6	−1.01	0.07
Del Rio	USNM 6524	6	−0.97	0.10
IIF average			*−0.99*	*0.13*
IIIE				
Willow Creek	Münster	5	−0.43	0.17
Paneth's Iron	BM 2005, M199	2	−0.53	0.13
Burlington	USNM 978	4	−0.53	0.07
Coopertown	USNM 1003	5	−0.54	0.20
IIIE average			*−0.51*	*0.09*
IIIF				
Klamath Falls	ME 2789	2	−1.06	0.13
Clark County	Münster	6	−0.93	0.04
Oakley*	USNM 780	5	−0.80	0.03
IIIF average			*−0.93*	*0.26*
Low exposure IIIF average			*−0.99*	*0.13*

[a] Data are normalized to ^{99}Ru/^{101}Ru = 0.7450754 (Chen et al., 2010). Uncertainties for individual samples are as in Table 1. Uncertainties for group means are the 2SD of standards ($N < 3$) or samples ($N = 3$), or the 95% confidence interval ($N \geq 4$). For Wiley, the uncertainty is the 2SD of duplicate measurements.

(ε^{94}Mo ~ 1.2; ε^{100}Ru ~ -1.0). The IIC irons have a Mo isotopic composition that is significantly different from the other CC irons (ε^{94}Mo $= 2.25 \pm 0.10$; 95% CI), but a Ru isotopic composition that is identical within uncertainty (ε^{100}Ru $= -1.04 \pm 0.05$; 2SD). Finally, a IIC iron meteorite, Wiley, has an ε^{94}Mo $= 3.42 \pm 0.07$ and an ε^{100}Ru $= -1.07 \pm 0.08$ (2SD). Wiley has the largest Mo isotope anomaly yet measured for an iron meteorite (Kruijer et al., 2017), but a similar Ru isotopic composition to the other CC irons. The small measured CRE effect on ε^{196}Pt, along with the shared ε^{100}Ru value of Wiley and other CC irons, indicates that the large Mo isotope anomaly is not due to CRE. Additionally, the ε^{183}W of Wiley is distinct from IIC irons (Kruijer et al., 2017), and the relative abundances of its highly siderophile elements suggest that it and the IIC irons crystallized from different parental melts (Tornabene et al., 2019). Therefore, it is likely that Wiley originated on a different parent body, and in a different nebular reservoir, than the IIC group.

4. Discussion

4.1. Comparison between the NC and CC reservoirs

4.1.1. Mo-Ru cosmic correlation

Dauphas et al. (2004) first identified that Mo and Ru isotope anomalies, which both reflect variable deficits in the s-process iso-
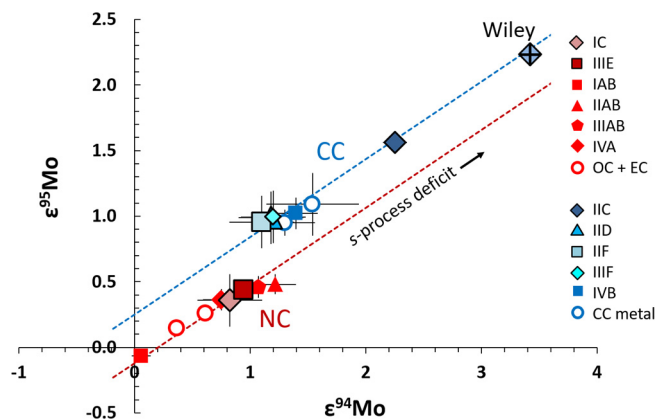

Fig. 1. ε^{94}Mo vs. ε^{95}Mo, illustrating the dichotomy between NC (in red) and CC (in blue) meteorites (Budde et al., 2016; Poole et al., 2017; Worsham et al., 2017). Symbols outlined in black denote rare iron meteorite groups examined in this work (data from this study and Kruijer et al., 2017). Members from both suites fall along theoretical s-process mixing lines between an s-process component and an s-process depleted component (Dauphas et al., 2004; Lugaro et al., 2003). The mixing lines for both suites are offset from the origin to align with the data. Other literature data are from Burkhardt et al. (2011), Render et al. (2017), Poole et al. (2017), and Bermingham et al. (2018). The offset between these lines cannot be accounted for by s-process variability but appears to reflect a relative enrichment of r- (and p-) process isotopes in the CC reservoir (Budde et al., 2016; Poole et al., 2017; Worsham et al., 2017; Bermingham et al., 2018). (For interpretation of the colors in the figures, the reader is referred to the web version of this article.)

topes, are correlated in what are now known as NC irons and the IVB group. This linear relationship has been interpreted as two-component mixing between an s-enriched and an s-depleted endmember and taken as evidence that Mo and Ru are hosted in a common presolar carrier or a few similar carriers. Notably, this relationship is linear because the s-process endmember is isotopically very different from the bulk meteorites, such that the curved mixing line appears linear in the relevant range.

In agreement with previous work (Dauphas et al., 2004; Fischer-Gödde et al., 2015; Bermingham et al., 2018), the ε^iMo and ε^{100}Ru compositions of NC iron meteorite groups define a roughly linear relationship (Figs. 2a, SM1). The slopes of the linear regressions through the NC irons on plots of ε^iMo vs. ε^{100}Ru are in good agreement with a theoretical s-process mixing line (calculated as in Dauphas et al., 2004). However, when CC irons are considered together, some plot well off the theoretical s-process mixing line on plots of ε^{92}Mo and ε^{94}Mo vs. ε^{100}Ru. Primarily these are the IIC irons and Wiley, which plot to the right of the reference line. This is also true when other Mo isotopes are plotted vs. ε^{100}Ru (Fig. SM1). It is also notable that IVB irons and other CC irons with similar isotopic compositions (the IID, IIF, and IIIF groups and chondrite metals; hereafter, the "CC cluster") plots slightly to the left of the reference line on plots of ε^{92}Mo and ε^{94}Mo vs. ε^{100}Ru. Cosmic ray exposure cannot explain why the IID, IIF, and IIIF groups fall to the left of the reference line, as most of the irons examined here were not exposed to high neutron fluence (Table 1), although this may explain why the IVB group does (See SM). The different relative abundances of p- and r-process isotopes defining the NC-CC dichotomy is most evident when p-process isotopes are included in plots (e.g., Fig. 1). For this reason, the CC cluster falls to the left of the theoretical line on plots of ε^{92}Mo and ε^{94}Mo vs. ε^{100}Ru, but when other Mo isotopes are plotted, the CC cluster falls closer to or on the theoretical s-process reference lines (Bermingham et al., 2018, Fig. SM1). This indicates that, like the IIC irons and Wiley, the CC cluster likely deviates from the NC array and cannot be accounted for by a pure s-process deficit.

Most importantly, the CC meteorites collectively exhibit variable Mo isotopic compositions, but uniform ε^{100}Ru. Thus, no
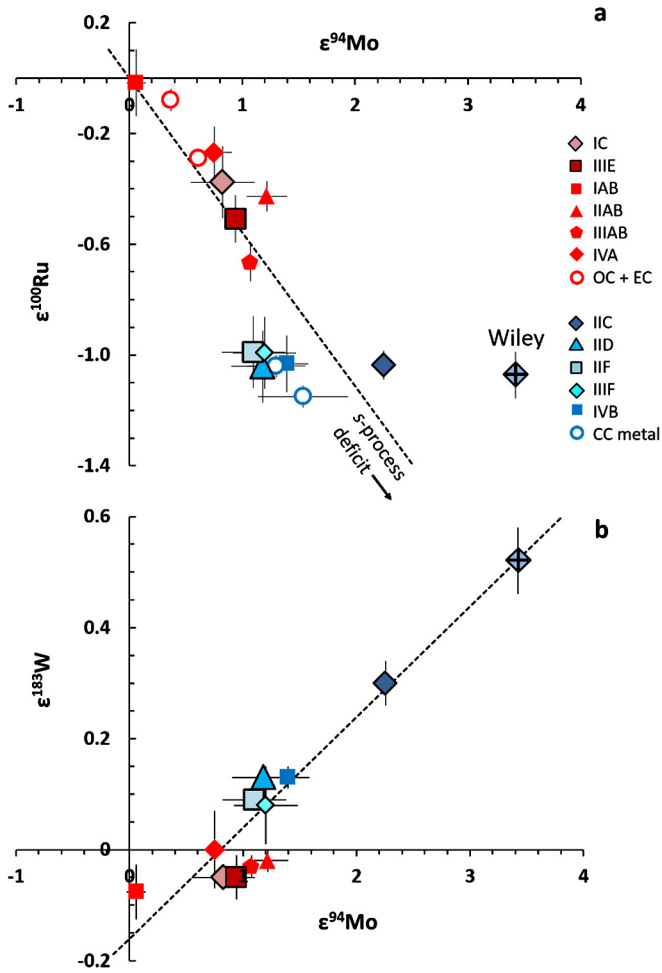
Fig. 2. ε^{94}Mo vs. ε^{100}Ru (a) and ε^{94}Mo vs. ε^{183}W (b) for various meteorite groups. Symbols outlined in black denote data for rare iron meteorite groups from this work. NC and CC meteorite groups are shown in red and blue, respectively. ε^{183}W data are from Kruijer et al. (2017), Kruijer et al. (2014a), and Worsham et al. (2017) and, for the rare iron groups, were obtained from the same sample set as Ru and Mo. Other literature data are from Chen et al. (2010), Burkhardt et al. (2011), Fischer-Gödde et al. (2015), Fischer-Gödde and Kleine (2017), Render et al. (2017), Poole et al. (2017), Worsham et al. (2017), and Bermingham et al. (2018). Also shown is an *s*-process mixing line, as in Fig. 1 (Dauphas et al., 2004; calculated using the same curvature coefficient used by those authors, which were estimated from Arlandini et al., 1999, and SiC compositions reported by Lugaro et al., 2003 and Savina et al., 2004). In (b) the *s*-process composition from Arlandini et al. (1999) was used to calculate the line, which is offset from the origin to align with the CC irons.

single linear correlation can be regressed through all the data. This non-linearity is not due to incomplete digestion of presolar phases in different pieces used for Mo and Ru analyses, as is a concern for unequilibrated chondrites, because these iron meteorites originated in equilibrated, differentiated parent bodies. Further, it is unlikely that differentiation or other parent body processes decoupled Ru from Mo in CC irons. This is because carbonaceous chondrites also have variable Mo isotopic compositions but ε^{100}Ru values which cluster around -0.9, although they vary over a range of -0.3 to -1.5 ε^{100}Ru (Fischer-Gödde et al., 2015; Fischer-Gödde and Kleine, 2017). As this isotopic variability is also seen within carbonaceous chondrite groups, it is likely due to sampling effects (Fischer-Gödde and Kleine, 2017). For this reason, we suspect that the processes that acted on the sampling scale are responsible for the entire isotopic range of carbonaceous chondrites, and that the average value of -0.9 ε^{100}Ru is representative of bulk carbonaceous chondrites, consistent with the uniform composition of iron meteorites (-1 ε^{100}Ru).

Some deviations from a single linear regression may be due to mixing of endmembers having variable Mo/Ru, which would change the curvature of the mixing line(s) (Dauphas et al., 2004). However, if this were exclusively the cause, it is surprising that these deviations are restricted to the CC suite. Moreover, the variable Mo isotopic compositions and restricted Ru isotopic compositions of the CC irons cannot be explained this way, but rather indicate that Mo and Ru were decoupled in the CC suite, either because Mo and Ru were hosted in different presolar phases from one another in the CC reservoir, and/or because processing of the presolar hosts of Mo and Ru only modified Mo (Fischer-Gödde et al., 2015). Regardless of the cause, however, it appears that the Mo-Ru correlation is not reflected in the CC irons, indicating that the nucleosynthetic heterogeneities in the NC and CC reservoirs did not originate in the same way, or under the same conditions.

4.1.2. Comparison to ^{183}W isotope anomalies

To investigate what presolar carriers or conditions were different between the two reservoirs, we compared the isotopic characteristics of Mo and Ru to those of W. Like Mo and Ru, W exhibits nucleosynthetic heterogeneity and is siderophile, refractory, and redox sensitive. Until recently, no nucleosynthetic ^{183}W isotope anomalies had been identified in bulk iron meteorites, apart from the IID and IVB iron meteorites (e.g., Qin et al., 2008; Kruijer et al., 2013). Burkhardt et al. (2012b) reported W isotope anomalies in Murchison leachates, which were broadly correlated with the corresponding Mo isotope anomalies. As with Mo and Ru, this suggests that Mo and W may be hosted in similar presolar carriers. However, Burkhardt et al. (2012b) also observed that the large Mo isotope variations among bulk meteorites are not observed for W, indicating that the two isotope systems were decoupled in the precursors of bulk meteorites. Notably, the only CC irons considered in that work were IVB irons.

The Mo and W data reported by Kruijer et al. (2017), supplemented here with new Mo data for a larger set of CC irons, show that large ε^{183}W isotope anomalies are observed in the CC irons, which are correlated with ε^iMo (Fig. 2b), in contrast to ε^iMo vs. ε^{100}Ru. The slope of the linear relationship among CC irons is in good agreement with that of the theoretical *s*-process mixing line of Arlandini et al. (1999). Thus, ^{183}W nucleosynthetic anomalies in the CC suite likely reflect variable deficits in the *s*-process W isotopes. In contrast to correlated ε^iMo and ε^{100}Ru in the NC irons, however, isotope ratios of ε^iMo and ε^{183}W are not correlated in the NC suite. The lack of ^{183}W isotope anomalies corresponding with Mo isotope anomalies among NC meteorites indicates that Mo and W are decoupled in those irons, which is generally consistent with the conclusion of Burkhardt et al. (2012b).

The observation that W shows no nucleosynthetic heterogeneity in the NC reservoir, and Ru is uniform in the CC reservoir, suggests that both reservoirs were well mixed at some stage. However, both reservoirs are also characterized by variable *s*-process deficits in Mo and either Ru or W. These seemingly conflicting observations can be reconciled if it is assumed that the reservoirs were each initially isotopically homogeneous (with regard to the distribution of *s*-process carriers), and the *s*-process variations were generated as a secondary feature of each reservoir. This relies on the assumption, however, that Mo, Ru, and W were hosted in similar *s*-process carriers in both reservoirs. Alternatively, the contrasting behaviors of Ru and W relative to Mo may suggest that at least two types of *s*-process carriers existed hosting either Mo-Ru (in the NC reservoir) or Mo-W (in the CC reservoir). However, perhaps except for a hypothesized component – the addition of which may have established the NC-CC dichotomy (as discussed below) – there is little reason to suspect that a specific carrier was present within one reservoir and not the other, as mixing evidently erased the large-scale variations among presolar grains in bulk meteorites. It is

Table 3

Molybdenum isotope data for rare iron meteorite groups. The data are not corrected for CRE exposure. Where irons with $\varepsilon^{196}Pt \geq 0.13$ were not included in the group mean, a low-exposure mean is given. The samples characterized by high exposure are denoted with an asterisk.

Meteorite	Collection (No.)	N	$\varepsilon^{92}Mo$[a]	±	$\varepsilon^{94}Mo$	±	$\varepsilon^{95}Mo$	±	$\varepsilon^{97}Mo$	±	$\varepsilon^{100}Mo$	±
IC												
Chihuahua City[b]	BM 1959, 1011	8	0.96	0.12	0.86	0.08	0.34	0.07	0.20	0.08	0.27	0.13
Arispe*	ME 1011	5	0.77	0.20	0.75	0.14	0.21	0.10	0.14	0.07	0.27	0.07
Bendego*	ME 6	5	0.83	0.07	0.83	0.13	0.26	0.06	0.23	0.11	0.31	0.18
Mount Dooling	USNM 5713	4	0.80	0.18	0.80	0.13	0.38	0.08	0.26	0.04	0.16	0.13
Murnpeowie[b]*	BM 2005, M179	8	1.16	0.20	1.11	0.20	0.41	0.05	0.27	0.05	0.37	0.08
IC average			*0.90*	*0.20*	*0.83*	*0.18*	*0.36*	*0.10*	*0.22*	*0.06*	*0.27*	*0.09*
Low exposure IC average			*0.88*	*0.39*	*0.83*	*0.28*	*0.36*	*0.20*	*0.23*	*0.14*	*0.21*	*0.23*
IIC												
Kumerina[b]	BM 1938, 220	8	2.91	0.28	2.34	0.18	1.50	0.08	0.79	0.10	0.92	0.09
Kumerina (replicate)	BM 1938, 220	5	2.90	0.20	2.27	0.15	1.59	0.08	0.80	0.08	0.85	0.13
Perryville	USNM 428	6	2.89	0.13	2.27	0.11	1.59	0.07	0.83	0.03	0.85	0.08
Ballinoo[b]	ME 980	8	2.76	0.13	2.19	0.10	1.60	0.09	0.89	0.09	1.01	0.10
Unter-Mässing	Münster	5	2.87	0.36	2.19	0.27	1.54	0.13	0.83	0.09	0.99	0.23
IIC average			*2.87*	*0.10*	*2.25*	*0.10*	*1.56*	*0.07*	*0.83*	*0.07*	*0.93*	*0.12*
Wiley[b]	BM 1959, 914	8	4.14	0.22	3.39	0.13	2.19	0.11	1.19	0.11	1.54	0.14
Wiley (replicate)	BM 1959, 914	3	4.28	0.39	3.45	0.28	2.24	0.20	1.26	0.14	1.45	0.23
Wiley (replicate)	BM 1959, 914	5	4.36	0.28	3.44	0.21	2.27	0.06	1.21	0.08	1.43	0.08
Wiley average			*4.26*	*0.22*	*3.42*	*0.07*	*2.23*	*0.08*	*1.22*	*0.07*	*1.47*	*0.12*
IID												
Bridgewater[b]	ME 1895	7	1.63	0.10	1.16	0.16	0.96	0.15	0.51	0.12	0.67	0.17
N'kandhla	BM 1921, 17	5	1.71	0.15	1.20	0.14	1.02	0.03	0.50	0.03	0.59	0.07
IID average			*1.67*	*0.39*	*1.18*	*0.28*	*0.99*	*0.20*	*0.51*	*0.14*	*0.63*	*0.23*
IIF												
Monahans[b]	BM 1959, 910	8	1.50	0.21	1.11	0.13	0.94	0.08	0.50	0.08	0.63	0.13
Del Rio	USNM 6524	4	1.54	0.22	1.09	0.10	0.97	0.06	0.52	0.01	0.61	0.10
IIF average			*1.52*	*0.39*	*1.10*	*0.28*	*0.96*	*0.20*	*0.51*	*0.14*	*0.62*	*0.23*
IIIE												
Willow Creek	Münster	5	1.10	0.30	0.94	0.23	0.41	0.11	0.24	0.10	0.28	0.17
Kokstad[1]*	ME 1015	8	0.98	0.17	0.86	0.14	0.33	0.13	0.26	0.09	0.28	0.08
Colonia Obreira[b]	ME 2871	8	1.03	1.36	0.97	0.16	0.35	0.09	0.25	0.14	0.35	0.12
Staunton[b]	BM 1955, M239	8	1.02	0.16	0.95	0.10	0.41	0.11	0.30	0.08	0.39	0.11
Paneth's iron[b]	BM 2005, M199	8	1.09	0.15	0.93	0.20	0.42	0.07	0.35	0.05	0.37	0.12
Burlington	USNM 978	4	1.06	0.26	0.95	0.11	0.52	0.11	0.34	0.07	0.16	0.02
Coopertown	USNM 1003	4	0.98	0.32	0.91	0.28	0.51	0.10	0.29	0.06	0.16	0.15
IIIE average			*1.04*	*0.04*	*0.93*	*0.03*	*0.42*	*0.07*	*0.29*	*0.04*	*0.28*	*0.09*
Low exposure IIIE average			*1.05*	*0.05*	*0.94*	*0.02*	*0.44*	*0.07*	*0.29*	*0.05*	*0.28*	*0.11*
IIIF												
Klamath Falls[b]	ME 2789	8	1.70	0.18	1.20	0.18	0.98	0.06	0.56	0.11	0.62	0.09
Clark County[b]	BM 1959, 949	6	1.45	0.23	1.20	0.17	1.00	0.06	0.54	0.04	0.59	0.23
Oakley*	USNM 780	6	1.31	0.12	1.01	0.09	0.83	0.13	0.54	0.11	0.56	0.07
IIIF average			*1.48*	*0.39*	*1.13*	*0.22*	*0.94*	*0.19*	*0.55*	*0.02*	*0.59*	*0.06*
Low exposure IIIF average			*1.57*	*0.39*	*1.20*	*0.28*	*0.99*	*0.20*	*0.55*	*0.14*	*0.61*	*0.23*

[a] Data are normalized to $^{98}Mo/^{96}Mo = 1.453173$ (Lu and Masuda, 1994). Uncertainties are as in Tables 1 and 2.
[b] Data from Kruijer et al. (2017).

considered more likely that both reservoirs had similar abundances of the same *s*-process carriers and that processing under distinct conditions led to the observed differences between the Mo-Ru-W relationships in iron meteorites.

4.2. Implications for the evolution of the NC and CC reservoirs

4.2.1. Establishment of the NC and CC reservoirs

The Mo isotope dichotomy was suggested to result from addition of *r*-process enriched material to the CC reservoir (Budde et al., 2016; Worsham et al., 2017), or preferential processing of *p*-process enriched carriers (Poole et al., 2017; discussed below). To account for the observation that some calcium-aluminum-rich inclusions (CAIs – some of the earliest solids formed in the solar system) have Mo isotopic signatures with stronger *r*-process enrichments than CC meteorites (Burkhardt et al., 2011; Brennecka et al., 2013), Nanne et al. (2019) suggested that the early disk, which formed by rapid viscous spreading of early infalling material from the molecular cloud, was enriched in *r*-process nuclides, and that CAIs formed from this material. After the formation of *r*-enriched CAIs, the composition of the infalling material shifted

to an *r*-depleted (NC-like) composition. This material mixed within the disk with the original *r*-process enriched material until the reservoirs were physically separated, potentially by the growth of Jupiter, which set the distinct compositions of the reservoirs and resulted in the CC reservoir having an intermediate composition between the NC and *r*-enriched components (Kruijer et al., 2017; Nanne et al., 2019).

Two-component mixing calculations between NC compositions and type B CAIs reveal that mixing between these compositions is consistent with the isotopic characteristics of most CC irons, in support of the Nanne et al. (2019) model (Fig. 3). Because the CC reservoir represents a mixture of both components, the later-added *r*-depleted component was present in both reservoirs (though concentrated in the NC reservoir). Therefore, processing of presolar materials constituting these components under the same conditions in each reservoir would not be expected to generate the observed differences in, and reciprocal nature of, the Mo-Ru and Mo-W relationships (i.e., coupled Mo-Ru may be expected in both reservoirs, which is not observed). To facilitate the following discussion, which is primarily concerned with the production of the contrasting *s*-process variations within each reservoir, we will fol-

low the model of Nanne et al. (2019), although the interpretations here are not dependent on how the reservoirs were established.

4.2.2. Initial homogeneity within the two reservoirs and evidence for thermal processing

The first suggestion that nucleosynthetic heterogeneity amongst bulk meteorites resulted from variable processing of presolar materials expanded on the observation that the abundances of certain presolar phases in chondrites was related to the type of chondrite and the degree of metamorphism (e.g., Huss et al., 2003). Trinquier et al. (2009) proposed this mechanism to account for the observed correlation of Ti isotopes, which are made by different nucleosynthetic processes, in bulk meteorites.

The thermal processing model assumes that the relative proportions of different presolar materials were initially the same throughout the protoplanetary disk due to turbulent mixing, resulting in an isotopically homogeneous disk (e.g., Trinquier et al., 2009). It is now known that the NC and CC reservoirs were isotopically distinct, but within each reservoir, turbulent mixing may have resulted in isotopic homogeneity. This supposed homogeneity was not chemical in nature (i.e., not due to thermal processing), but was due to efficient mechanical mixing of the dust. Mechanical mixing is supported by the observation that all chondrites have identical nucleosynthetic Os isotope compositions, despite the evidence that isotopically distinct presolar carriers of Os are revealed by chondrite leachates (Yokoyama et al., 2010).

Heretofore, the lack of primary nucleosynthetic anomalies in heavy elements, such as Os, in bulk meteorites from either reservoir has argued for isotopic homogeneity within the disk and against inherited nucleosynthetic heterogeneity (e.g., Walker, 2012). The counterargument is that most of the isotopically homogeneous heavy elements are produced primarily by the r-process and may be hosted in different carriers, such that these elements may not reflect inherited s-process heterogeneity. However, several lines of evidence suggest that s-process nuclides were also initially homogeneously distributed within each reservoir. First, the results of this study demonstrate that W and Ru, both produced in part by the s-process, were isotopically uniform in one reservoir. Further, the uniform Ru isotopic composition in the CC reservoir, combined with the presence of s-process Ru variations in the NC reservoir, suggests that, like the CC reservoir, the NC reservoir was isotopically homogeneous prior to the generation of the s-process variability within it. This is supported by the W isotopic homogeneity in the NC reservoir. The same argument can be made for initial W isotopic homogeneity in the CC reservoir.

Second, initial isotopic homogeneity in each reservoir is supported by the Mo isotope dichotomy, because CC and NC meteorites fall on two parallel regressions on plots of ε^{92}Mo and ε^{94}Mo vs. ε^{i}Mo (Budde et al., 2019), reflecting identical s-process variations in each reservoir (Fig. 1). This indicates that the relative enrichments of r- and p-process isotopes to s-process isotopes are distinct between the two reservoirs, but approximately constant within them; otherwise, the regressions would have significantly different slopes, or there would be scatter about the regressions. Therefore, the r- and p-process component(s) in each reservoir must have been homogeneously distributed. It is difficult to envision how these constant relative enrichments of r- and p-process to s-process isotopes could be achieved if the s-process variations were pre-existing and maintained during the establishment of the two reservoirs. However, if each reservoir had distinct, but homogeneous isotopic compositions, the pure s-process variations could easily be explained if they were generated independently after the two reservoirs were established.

Finally, the preponderance of chemically diverse irons and chondritic metals in the CC cluster suggests widespread homogenization of the precursor materials in the CC reservoir. This was first concluded by Bermingham et al. (2018), who noted that ungrouped irons originating from three chemically diverse parent bodies cluster with the IVB group on plots of ε^{i}Mo vs. ε^{100}Ru. Including meteorites that have Mo isotopic compositions within uncertainty of the IVB group, and the rare groups reported here, at least 15 parent bodies have tightly clustered Mo and Ru isotopic compositions (Fig. 4). The variety and number of parent bodies, which include differentiated, undifferentiated, volatile-depleted, and volatile-enriched parent bodies, suggests that they formed over a range of heliocentric distances and over an extended period of time. This would require that a large portion of the disk had a homogeneous isotopic composition when the parent bodies representing the CC cluster formed. If this homogenized region was representative of the CC reservoir, then it implies that the isotopic composition of the CC cluster of meteorites is close to the initial composition of the CC reservoir as a whole and that chemical or thermal processing of the precursor materials is responsible for generating more isotopically anomalous compositions (e.g., Wiley).

Given the isotopic homogeneity of both r- and s-process synthesized elements in both reservoirs, the parallel trends of the NC and CC suites on Mo isotope plots, and the clustered isotopic compositions of most CC irons, it is likely that both reservoirs were initially isotopically homogeneous and that processing of presolar material in both the NC and CC reservoirs generated the s-process nucleosynthetic heterogeneity at the bulk meteorite scale. Moreover, the contrasting behaviors of Ru and W relative to Mo in the NC and CC reservoirs likely require that processing occurred under distinct conditions in the two reservoirs.

To summarize this mechanism generally, thermal processing of dust in an isotopically homogenized portion of the disk (i.e., within either the NC or the CC reservoir) may have destroyed some isotopically anomalous presolar phase(s), vaporizing certain constituent elements (but likely not all). The isotopically anomalous vapor would be removed from the dust, due to settling, gas drag, and radial forces, leaving a complimentary isotopically anomalous residue from which planetesimals could accrete. In an environment where this type of processing occurred, an element could retain isotopic homogeneity if its host(s) was not affected, or if it was not lost from the system. Thus, whether an element exhibits nucleosynthetic heterogeneity depends, in part, on the durability of its presolar host(s) and on the volatility of that element. The volatility of a given element is dependent on many factors, including the redox conditions and its proclivity to form volatile molecular species. For example, under certain nebular conditions, thermodynamic calculations suggest that Mo and W readily form volatile oxides, whereas Ru does not (Fegley and Palme, 1985). Notably, if thermal processing via vaporization occurred, large-scale elemental fractionations would not be expected, as only small degrees of partial evaporation of an element from anomalous presolar material would be necessary to create the observed nucleosynthetic effects.

Given the results presented here, a model explaining the relative isotopic behaviors of Mo, Ru, and W must satisfy the requirements that Mo and Ru behaved similarly in the NC reservoir, and Mo and W behaved similarly in the CC reservoir. This can be accomplished by appealing to different redox conditions between the two reservoirs. Using 50% condensation temperatures (T_C) as a proxy for relative volatilities under reducing conditions, Mo and Ru have lower 50% T_C than W (1587, 1546, and 1790 K, respectively – Lodders, 2003). Similarly, calculations done by Fegley and Palme (1985) show that Mo and Ru may be depleted in a W(Re, Os) alloy formed via fractional condensation, whereas the complementary gas would be enriched in Mo and Ru, and depleted in W. Indeed, refractory metal nuggets (RMNs), some of which likely represent primary condensates from the solar nebula, have, on average, lower CI-normalized abundances of Ru and Mo relative to W (Berg et al., 2009; Daly et al., 2017). This indicates that W may

be condensed from the gas at higher temperatures, and incorporated into RMNs condensed at those temperatures, more readily than Mo and Ru. The corollary is that, as metals, Mo and Ru may be volatilized under reducing conditions more readily than W from their presolar hosts, and W may stay in the residue if it remains refractory during this process. By contrast, Mo and W form volatile oxides more readily than Ru (Fegley and Palme, 1985). Thus, under oxidizing conditions, Mo and W can form oxides which may be volatilized from their presolar hosts, whereas Ru may remain in the residue.

The disparate Mo-Ru-W isotope systematics in the NC and CC reservoirs can, therefore, be accounted for by thermal processing of presolar material under relatively reducing conditions in the NC reservoir, and under oxidizing conditions in the CC reservoir. This is also broadly consistent with the bulk chemistry of chondrites and iron meteorites. The CC suite includes more volatile-rich carbonaceous chondrites (although some CC iron meteorite groups are volatile-depleted), and the NC reservoir includes volatile-depleted and more reduced enstatite and ordinary chondrites. In the case of iron meteorites, it has been suggested that the CC iron groups have higher Ni and refractory siderophile element abundances due to the more oxidized conditions of their core formation relative to NC irons (Rubin, 2018).

Given the chronological evidence that the NC and CC reservoirs were physically separated for an extended period of time (Kruijer et al., 2017), the different locations of the two reservoirs likely contributed to the prevailing thermal and redox conditions. Warren (2011) and Kruijer et al. (2017) suggested that the CC and NC reservoirs were in the outer and inner solar system, respectively, which is consistent with the implication of the present study that the CC reservoir was generally more oxidizing than the NC reservoir. In addition to the bulk chemistry of CC and NC meteorites, ratios of $^{15}N/^{14}N$ for iron meteorites support this conclusion as well. Füri and Marty (2015) argued that enrichments in ^{15}N are generally associated with the presence of organics and ices, and ^{15}N enrichments may increase with heliocentric distance (although there are exceptions – e.g., Jupiter). Iron meteorites that are classified as CC irons here and elsewhere are enriched in ^{15}N ($\delta^{15}N$ ranges from +3 to +150‰), whereas irons that are classified as NC meteorites are typically depleted in ^{15}N ($\delta^{15}N$ ranges from −90 to −3‰ – Prombo and Clayton, 1993). Therefore, if the CC reservoir was in the outer solar system, hydration of the dust or the presence of ice in the dust may have led to the more oxidizing conditions (Fegley and Palme, 1985; Fedkin and Grossman, 2016).

4.2.3. Model for the origin of nucleosynthetic heterogeneity

Based on the relative isotopic characteristics of Mo, Ru, and W in the NC and CC reservoirs, a simplified illustration of the thermal/chemical processing discussed above and the collateral isotopic effects among Mo, Ru, and W isotopes is presented here (Fig. 3). This illustration provides only one example, but other models are possible.

The initial composition of the disk is taken as that of Nanne et al. (2019) (point A in Fig. 3), which is equivalent to the composition of type B CAIs. As discussed in section 4.2.1 and Nanne et al. (2019), the two reservoirs were likely established when NC-like material was mixed into the disk (point B). Note that these components represent the characteristic compositions of two bulk disk reservoirs and are, therefore, not hosted in any specific presolar phase (Nanne et al., 2019). Moreover, the approximately constant relative abundances of *r*- and *p*-process isotopes within the reservoirs indicates that the *r*- and *p*-process Mo isotopes are also not hosted in specific carriers, but represent a homogenized nebular component (Dauphas et al., 2002b) in each reservoir (Budde et al., 2019).
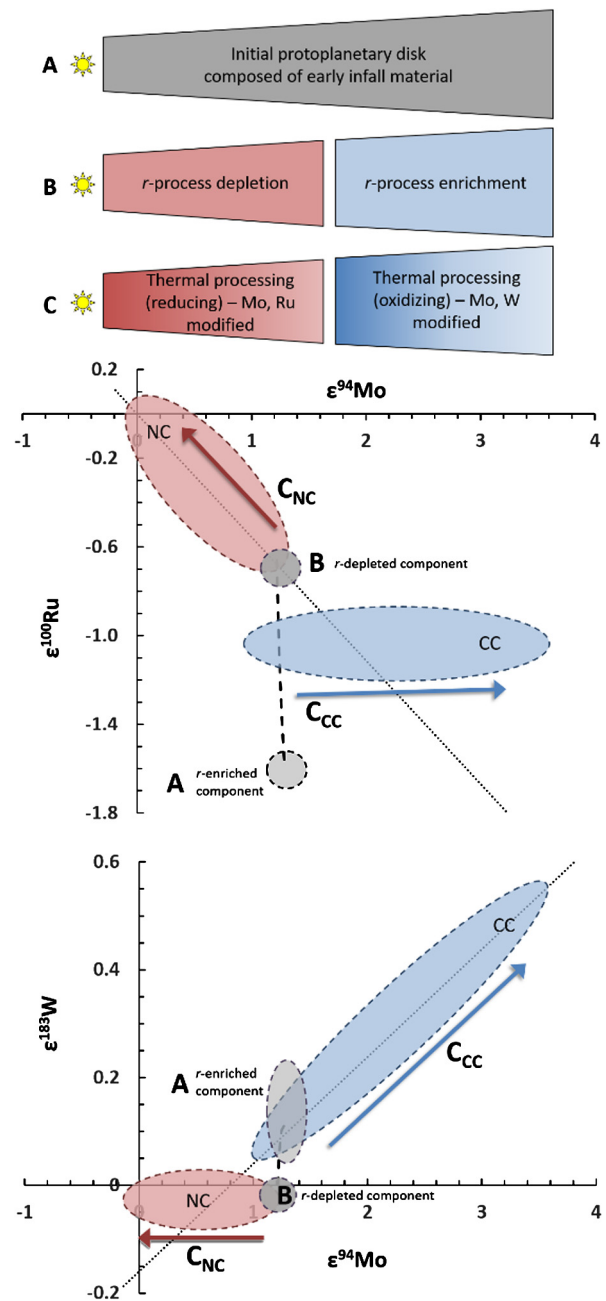
Fig. 3. Schematic diagram for the generation of Mo, Ru, and W nucleosynthetic heterogeneity in the NC and CC reservoirs in the protoplanetary disk (top of figure), and possible collateral isotopic effects in Mo, Ru, and W. Time progresses from A to C, which correspond with one another on the top and bottom portions of the figure. The dotted line is the *s*-process mixing line as in Fig. 2. Also shown are two-component mixing lines (dashed lines) between the compositions of type B CAIs, which represent an *r*-process enriched component (point A; Nanne et al., 2019) and an arbitrary NC composition (near the composition of IIIAB iron meteorites and corresponding to point B). See section 4.2.3 for details. Type B CAI data are from Chen et al. (2010), Burkhardt et al. (2011), Burkhardt et al. (2012a), and Kruijer et al. (2014b). We note that the large variance among published $\varepsilon^{183}W$ values for type B CAIs is schematically indicated by the larger field of the *r*-enriched component (A), but the variance is not fully represented here. Specifically, the CAI data from Burkhardt et al. (2012a) and Kruijer et al. (2014b) range from −0.17 to 0.52 $\varepsilon^{183}W$. Higher values are more *r*-enriched/*s*-depleted. If the higher values are used, W compositions in CC samples can be reproduced with similar mixing proportions to those obtained when CC Mo and Ru compositions are reproduced.

Prior to the accretion of most meteorite parent bodies, thermal processing in the NC reservoir under relatively reducing conditions may have destroyed thermally labile, homogenized nebular dust
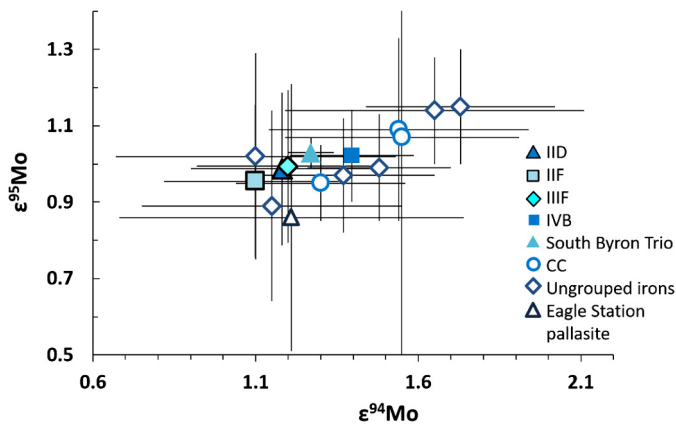
Fig. 4. Mo isotope data for diverse meteorites and meteorite groups having similar compositions to the IVB, IID, IIF, and IIIF iron meteorite groups. Data are from Dauphas et al., 2002a (Grand Rapids, Eagle Station), Burkhardt et al., 2011 (Mbosi, Tafassasset, and Gujba), Burkhardt et al., 2014 (CK), Worsham et al., 2017 (Sombrerete), Bermingham et al., 2018 (Chinga, Dronino, Tishomingo), and Hilton et al., 2019 (South Byron Trio). Samples where Ru isotope data have been reported are also within uncertainty of the Ru isotopic composition of the IVB group.

(i.e., dust with an s-depletion and a relative enrichment in r- and p-process isotopes). Molybdenum and Ru may be preferentially volatilized from this r- and p-process enriched dust and separated from the residue, whereas W isotopes may remain in the residue in solar proportions. Essentially, this processing would concentrate any more robust presolar materials enriched in s-process nuclides, which would drive the Mo and Ru isotopic compositions toward less s-process depleted compositions (toward the terrestrial composition). In this scenario, the terrestrial composition represents the most thermally processed precursor materials yet sampled (as was also suggested by Burkhardt et al., 2012b and Poole et al., 2017) (Line C_{NC} in Fig. 3).

In the CC reservoir, the more oxidizing conditions may have resulted in the destruction of presolar carriers by oxidation, during which Mo and W formed volatile oxides and Ru stayed in the residue. To accommodate the evidence for an initially homogeneous composition of the CC reservoir near the CC cluster (Fig. 4), processing likely resulted in the loss of s-process isotopes from an s-process carrier, generating the more s-depleted Mo and W isotopic compositions of the IIC irons and Wiley (Line C_{CC} in Fig. 3).

New open questions include what the specific presolar phases involved in processing in each reservoir were. For example, Poole et al. (2017) argued for a model that is generally in agreement with that presented above and in Burkhardt et al. (2012b), where processing of p-process and r-process carriers resulted in decreasing s-process deficits with greater degrees of thermal processing. However, Poole et al. (2017) advocate for this type of processing in both the NC and CC reservoirs, with the exception that p-process isotopes were preferentially lost over r-process isotopes in CC irons due to physical differences between p- and r-process material. These authors also propose that this process is what established the two reservoirs, which is difficult to reconcile with the observation that the CC and NC reservoirs form two parallel s-process mixing lines on ε^iMo plots (Fig. 1; Budde et al., 2019). If the preferential loss of p-process isotopes in the CC reservoir occurred, it may have led to different slopes between the NC and CC irons.

Other open questions relate to the conditions at which evaporation of Mo, Ru, and W can occur and the actual temperatures, pressures, and oxidation states within different regions of the disk. Heating of the protoplanetary disk by irradiation and viscous friction likely resulted in temperatures ranging from 500-1500 K in the inner disk to 50-150 K in the outer disk (Boss, 1998). Transient heating events also evidently occurred, given that temperatures required for chondrule formation are 1500-2000 K (e.g., Boss, 1998).

These estimates of transient disk temperatures generally compare favorably with temperatures at which Mo, Ru, and W may evaporate. While likely not representative of the full temperature range at which this is possible, calculations by Fegley and Palme (1985) show coupled Mo and Ru behavior at ~1675 K and coupled Mo and W behavior between 1450–1650 K. In terms of redox conditions, Fegley and Palme (1985) showed that Mo and W may be coupled at H_2O/H_2 ratios of 10^{-2} to 10^{-1}, below which Mo and Ru may be coupled (the solar H_2O/H_2 ratio is 5×10^{-4}). Environments in which these conditions may be met include localized regions of dust/ice enrichment, especially if the dust is hydrated (e.g., Fegley and Palme, 1985; Fedkin and Grossman, 2016).

5. Conclusions

Combined Ru, Mo, and W isotope data for iron meteorites, including the first high-precision mass-independent Ru isotope data from the rare iron meteorite groups IIC, IIF, IIIE, and IIIF, reveal a distinct genetic heritage of CC and NC meteorites. This work, along with the work of Fischer-Gödde et al. (2015), Fischer-Gödde and Kleine (2017), and Bermingham et al. (2018) shows that CC iron meteorites, and potentially bulk carbonaceous chondrites, are likely restricted to an ε^{100}Ru of -1. When considered together, these data reveal decoupled Mo-Ru isotope systematics in the CC reservoir, in contrast to the coupled Mo-Ru systematics in the NC reservoir. Conversely, W and Mo are correlated in the CC suite, but not the NC suite. This new observation of the contrasting behaviors of Ru and W, relative to Mo, in the two reservoirs allows for constraining the distinct mechanisms and physical conditions under which nucleosynthetic heterogeneity was generated in the protoplanetary disk. The data presented here not only provide further evidence that thermal/chemical processing of presolar phases generated s-process nucleosynthetic heterogeneity, but it also demonstrates that the heterogeneity within the CC and NC reservoirs evolved under distinct redox conditions. Specifically, the prevailing conditions in the NC reservoir were likely more reducing than those in the more oxidized CC reservoir, consistent with the inferred location of these reservoirs inside and outside the orbit of Jupiter, respectively.

Appendix A. Supplementary material

Supplementary material related to this article can be found online at https://doi.org/10.1016/j.epsl.2019.06.001.

References

Arlandini, C., Käppeler, F., Wisshak, K., Gallino, R., Lugaro, M., Busso, M., Straniero, O., 1999. Neutron capture in low-mass asymptotic giant branch stars: cross sections and abundance signatures. Astrophys. J. 525, 886–900.

Berg, T., Maul, J., Schönhense, G., Marosits, E., Hoppe, P., Ott, U., Palme, H., 2009. Direct evidence for condensation in the early solar system and implications for nebular cooling rates. Astrophys. J. 702 (2), L172.

Bermingham, K.R., Worsham, E.A., Walker, R.J., 2018. New insights into Mo and Ru isotope variation in the nebula and terrestrial planet accretionary genetics. Earth Planet. Sci. Lett. 487, 221–229.

Birck, J.-L., Roy-Barman, M., Capmas, F., 1997. Re-Os isotopic measurements at the femtomole level in natural samples. Geostand. Newsl. 20, 9–27.

Boss, A.P., 1998. Temperatures in protoplanetary disks. Annu. Rev. Earth Planet. Sci. 26, 53–80.

Brennecka, G.A., Borg, L.E., Wadhwa, M., 2013. Evidence for supernova injection into the solar nebula and the decoupling of r-process nucleosynthesis. Proc. Natl. Acad. Sci. 110 (43), 17241–17246.

Budde, G., Burkhardt, C., Brennecka, G.A., Fischer-Gödde, M., Kruijer, T.S., Kleine, T., 2016. Molybdenum isotopic evidence for the origin of chondrules and a distinct genetic heritage of carbonaceous and non-carbonaceous meteorites. Earth Planet. Sci. Lett. 454, 293–303.

Budde, G., Burkhardt, C., Kleine, T., 2019. Molybdenum isotopic evidence for the late accretion of outer Solar System material to Earth. Nat. Astron. https://doi.org/10.1038/s41550-019-0779-y.

Burkhardt, C., Kleine, T., Oberli, F., Pack, A., Bourdon, B., Wieler, R., 2011. Molybdenum isotope anomalies in meteorites: constraints on solar nebula evolution and origin of the Earth. Earth Planet. Sci. Lett. 312, 390–400.

Burkhardt, C., Kleine, T., Dauphas, N., Wieler, R., 2012a. Nucleosynthetic tungsten isotope anomalies in acid leachates of the Murchison chondrite: implications for Hf-W chronometry. Astrophys. J. Lett. 753, L6.

Burkhardt, C., Kleine, T., Dauphas, N., Wieler, R., 2012b. Origin of isotopic heterogeneity in the solar nebula by thermal processing and mixing of nebular dust. Earth Planet. Sci. Lett. 357, 298–307.

Burkhardt, C., Hin, R.C., Kleine, T., Bourdon, B., 2014. Evidence for Mo isotope fractionation in the solar nebula and during planetary differentiation. Earth Planet. Sci. Lett. 391, 201–211.

Chen, J.H., Papanastassiou, D.A., Wasserburg, G.J., 2010. Ruthenium endemic isotope effects in chondrites and differentiated meteorites. Geochim. Cosmochim. Acta 74, 3851–3862.

Clayton, D.D., 1982. Cosmic chemical memory: a new astronomy. Q. J. R. Astron. Soc. 23, 174–212.

Daly, L., Bland, P.A., Dyl, K.A., Forman, L.V., Evans, K.A., Trimby, P.W., Moody, S., Yang, L., Liu, H., Ringer, S.P., Ryan, C.G., 2017. In situ analysis of Refractory Metal Nuggets in carbonaceous chondrites. Geochim. Cosmochim. Acta 216, 61–81.

Dauphas, N., Schauble, E.A., 2016. Mass fractionation laws, mass-independent effects, and isotopic anomalies. Annu. Rev. Earth Planet. Sci. 44, 709–783.

Dauphas, N., Marty, B., Reisberg, L., 2002a. Molybdenum evidence for inherited planetary scale isotope heterogeneity of the protosolar nebula. Astrophys. J. 565, 640–644.

Dauphas, N., Marty, B., Reisberg, L., 2002b. Molybdenum nucleosynthetic dichotomy revealed in primitive meteorites. Astrophys. J. 569, L139–L142.

Dauphas, N., Davis, A.M., Marty, B., Reisberg, L., 2004. The cosmic molybdenum-ruthenium isotope correlation. Earth Planet. Sci. Lett. 226, 465–475.

Dauphas, N., Remusat, L., Chen, J.H., Roskosz, M., Papanastassiou, D., Stodolna, J., Guan, Y., Ma, C., Eiler, J.M., 2010. Neutron-rich chromium isotope anomalies in supernova nanoparticles. Astrophys. J. 720, 1577–1591.

Fedkin, A.V., Grossman, L., 2016. Effects of dust enrichment on oxygen fugacity of cosmic gases. Meteorit. Planet. Sci. 51, 843–850.

Fegley Jr., B., Palme, H., 1985. Evidence for oxidizing conditions in the solar nebula from Mo and W depletions in refractory inclusions in carbonaceous chondrites. Earth Planet. Sci. Lett. 72, 311–326.

Fischer-Gödde, M., Burkhardt, C., Kruijer, T.S., Kleine, T., 2015. Ru isotope heterogeneity in the solar protoplanetary disk. Geochim. Cosmochim. Acta 168, 151–171.

Fischer-Gödde, M., Kleine, T., 2017. Ruthenium isotopic evidence for an inner solar system origin of the late veneer. Nature 541, 525–527.

Füri, E., Marty, B., 2015. Nitrogen isotope variations in the Solar System. Nat. Geosci. 8, 515–522.

Goderis, S., Brandon, A.D., Mayer, B., Humayun, M., 2015. s-Process Os isotope enrichment in ureilites by planetary processing. Earth Planet. Sci. Lett. 431, 110–118.

Hilton, C.D., Bermingham, K.R., Walker, R.J., McCoy, T.J., 2019. Genetics, crystallization sequence, and age of the South Byron Trio iron meteorites: new insights to carbonaceous chondrite (CC) type parent bodies. Geochim. Cosmochim. Acta 251, 217–228.

Huss, G.R., Meshik, A.P., Smith, J.B., Hohenberg, C.M., 2003. Presolar diamond, silicon carbide, and graphite in carbonaceous chondrites: implications for thermal processing in the solar nebula. Geochim. Cosmochim. Acta 67, 4823–4848.

Kruijer, T.S., Fischer-Gödde, M., Kleine, T., Sprung, P., Leya, I., Wieler, R., 2013. Neutron capture on Pt isotopes in iron meteorites and the Hf-W chronology of core formation in planetesimals. Earth Planet. Sci. Lett. 361, 162–172.

Kruijer, T.S., Touboul, M., Fischer-Gödde, M., Bermingham, K.R., Walker, R.J., Kleine, T., 2014a. Protracted core formation and rapid accretion of protoplanets. Science 344, 1150–1154.

Kruijer, T.S., Kleine, T., Fischer-Gödde, M., Burkhardt, C., Wieler, R., 2014b. Nucleosynthetic W isotope anomalies and the Hf-W chronometry of Ca–Al-rich inclusions. Earth Planet. Sci. Lett. 403, 317–327.

Kruijer, T.S., Burkhardt, C., Budde, G., Kleine, T., 2017. Age of Jupiter inferred from the distinct genetics and formation times of meteorites. Proc. Natl. Acad. Sci. USA 114 (26), 6712–6716.

Lodders, K., 2003. Solar System abundances and condensation temperatures of the elements. Astrophys. J. 59, 1220–1247.

Lu, Q., Masuda, A., 1994. The isotopic composition and atomic weight of molybdenum. Int. J. Mass Spectrom. Ion Process. 130, 65–72.

Lugaro, M., Davis, A.M., Gallino, R., Pellin, M.J., Straniero, O., Käppeler, F., 2003. Isotopic compositions of strontium, zirconium, molybdenum, and barium in single presolar SiC grains and asymptotic giant branch stars. Astrophys. J. 593, 486–508.

Nanne, J.A.M., Nimmo, F., Cuzzi, J.N., Kleine, T., 2019. Origin of the non-carbonaceous-carbonaceous meteorite dichotomy. Earth Planet. Sci. Lett. 511, 44–54.

Poole, G.M., Rehkämper, M., Coles, B.J., Goldberg, T., Smith, C.L., 2017. Nucleosynthetic molybdenum isotope anomalies in iron meteorites – new evidence for thermal processing of solar nebula material. Earth Planet. Sci. Lett. 473, 215–226.

Prombo, C.A., Clayton, R.N., 1993. Nitrogen isotopic compositions of iron meteorites. Geochim. Cosmochim. Acta 57, 3749–3761.

Qin, L., Dauphas, N., Wadhwa, M., Markowski, A., Gallino, R., Janney, P.E., Bouman, C., 2008. Tungsten nuclear anomalies in planetesimal cores. Astrophys. J. 674, 1234–1241.

Regelous, M., Elliott, T., Coath, C.D., 2008. Nickel isotope heterogeneity in the early Solar System. Earth Planet. Sci. Lett. 272, 330–338.

Rehkämper, M., Halliday, A.N., 1997. Development and application of new ion-exchange techniques for the separation of the platinum group and other siderophile elements from geological samples. Talanta 44, 663–672.

Render, J., Fischer-Gödde, M., Burkhardt, C., Kleine, T., 2017. The cosmic molybdenum-neodymium isotope correlation and the building material of the Earth. Geochem. Perspect. Lett. 3, 170–178.

Rubin, A.E., 2018. Carbonaceous and noncarbonaceous iron meteorites: differences in chemical, physical, and collective properties. Meteorit. Planet. Sci. 53 (11), 2357–2371.

Savina, M.R., Davis, A.M., Tripa, C.E., Pellin, M.J., Gallino, R., Lewis, R.S., Amari, S., 2004. Extinct technetium in silicon carbide stardust grains: implications for stellar nucleosynthesis. Science 303, 649–652.

Tornabene, H., Hilton, C.D., Ash, R.D., Walker, R.J., 2019. New insights to the genetics, age, and crystallization of group IIC iron meteorites. Lunar Planet. Sci. L, #1236 (abstr.). Lunar Planet. Inst., Houston.

Trinquier, A., Elliott, T., Ulfbeck, D., Coath, C., Krot, A.N., Bizzarro, M., 2009. Origin of nucleosynthetic isotope heterogeneity in the solar protoplanetary disk. Science 324, 374–376.

Walker, R.J., 2012. Evidence for homogeneous distribution of osmium in the protosolar nebula. Earth Planet. Sci. Lett. 351, 36–44.

Warren, P.H., 2011. Stable-isotopic anomalies and the accretionary assemblage of the Earth and Mars: a subordinate role for carbonaceous chondrites. Earth Planet. Sci. Lett. 311, 93–100.

Worsham, E.A., Bermingham, K.R., Walker, R.J., 2017. Characterizing cosmochemical materials with genetic affinities to the Earth: genetic and chronological diversity within the IAB iron meteorite complex. Earth Planet. Sci. Lett. 467, 157–166.

Yokoyama, T., Alexander, C.M.O'D., Walker, R.J., 2010. Osmium isotope anomalies in chondrites: results for acid residues and related leachates. Earth Planet. Sci. Lett. 291, 48–59.